INL/RPT-23-71531
Revision 0

Report on the Incorporation of Post-Irradiation Examination Results of Yttrium Hydride for Advanced Moderator Handbook

September 2023

M. Nedim Cinbiz, Joey A. Charboneau, Ian M. Hobbs, Jatuporn Burns, Scott C. Middlemas, Narayan Poudel, Tsvetoslav R. Pavlov, Glen C. Papaioannou, Thomas A. Johnson, Lance A. Hone, Rafael H. Garcia, Malwina A. Wilding, and Chase N. Taylor
Idaho National Laboratory

Idaho National Laboratory

INL is a U.S. Department of Energy National Laboratory operated by Battelle Energy Alliance, LLC

operated by Battelle Energy Alliance, LLC

INL/RPT-23-71531
Revision 0

Report on the Incorporation of Post-Irradiation Examination Results of Yttrium Hydride for Advanced Moderator Handbook

M. Nedim Cinbiz, Joey A. Charboneau, Ian M. Hobbs, Jatuporn Burns, Scott C. Middlemas, Narayan Poudel, Tsvetoslav R. Pavlov, Glen C. Papaioannou, Thomas A. Johnson, Lance A. Hone, Rafael H. Garcia, Malwina A. Wilding, and Chase N. Taylor
Idaho National Laboratory

September 2023

Idaho National Laboratory
Idaho Falls, Idaho 83415

http://www.inl.gov

Prepared for the
U.S. Department of Energy
Office of Nuclear Energy
Under DOE Idaho Operations Office
Contract DE-AC07-05ID14517

Page intentionally left blank

SUMMARY

Department of Energy's Microreactor Program provides fundamental data to enable the development of microreactors. For this reason, material-property data of critical materials for microreactor technologies are researched. Because substoichiometric yttrium dihydride (YH_x, where $x<2$) is considered as a potential solid neutron moderator, its material-property data has been combined in the Advanced Moderator Material Handbook, which includes thermodynamic and thermophysical properties of YH_x with the exception of irradiated material's properties due to limited post-irradiation examination (PIE).

To fill the knowledge gap for the irradiated YH_x, specimens and irradiation capsules were prepared at Los Alamos National Laboratory. Specimens were irradiated in the Advanced Test Reactor at Idaho National Laboratory (INL). PIE was performed at INL's Materials and Fuels Complex.

This report compiles the PIE results of irradiated YH_x specimens through fiscal years 2022 and 2023 (FY 22–23). [a] PIE data will be directly incorporated into new revisions of the Advanced Moderator Material Handbook.

The main takeaways include that (1) the geometrical stability and mechanical integrity of YH_x was intact with few exceptions after high-temperature (600–800°C) irradiations; (2) hydrogen content variation, due to manufacturing or irradiation in $YH_{x+,}$ caused visible surface discoloration, which is also related to the microstructural changes; (3) qualitative comparisons of PIE methods implied that hydrogen retention was significantly higher at 600°C than at 800°C; (4) thermal properties included signatures correlated with hydrogen loss or regain, (5) the importance of manufacturing readiness and initial as-manufactured specimens history was emphasized, and (6) the needs of targeted irradiations focusing on temperature and time parameters and very targeted PIE were specified.

[a] To incorporate data into Advanced Moderator Material Handbook, some sections, in particular the methods, are copied from the initial PIE report (Reference 3) that are already reported.

Acknowledgements

The authors are thankful to the Materials and Fuel Complex staff for the post-irradiation examination (PIE) activities and specimen transfers. They are indebted to Cad Christensen and John Stanek for the retrieval of the specimens from irradiation vehicles at the Hot Fuels Examination Facility. The authors also acknowledge Richard Farrar, who enabled specimen-management and critical PIE activities at the Analytical Research Laboratory. Thanks to Larry Greenwood from Pacific Northwest National Laboratory for conducting fluence-wire examinations. The patience of John Jackson (Idaho National Laboratory) is recognized by the authors.

CONTENTS

FIGURES

TABLES

ACRONYMS

ARL	Analytical Research Laboratory
ASTM	American Society of Testing and Materials
ATR	Advanced Test Reactor
BSE	Back-scattered electrons
CIC	Core internal changeout
DOE	Department of Energy
DSC	Differential scanning calorimetry
EBSD	Electron backscatter diffraction
EDS	Energy dispersive spectroscopy
FEA	Finite element analysis
FY	Fiscal year
GDS	Glow discharge optical emission spectroscopy
HFEF	Hot Fuels Examination Facility
IGF	Inert gas fusion
INL	Idaho National Laboratory
LANL	Los Alamos National Laboratory
LFA	Laser flash analysis
MH	Massive hydriging
MFC	Materials and Fuels Complex
MRP	Micro Reactor Program
NE	Nuclear Energy
NIST	National Institute of Standards and Technology
NRAD	Neutron Radiography Reactor
PIE	Post-irradiation examination
PM	Powder metallurgy
PNNL	Pacific Northwest National Laboratory
PRD	Push-rod dilatometry
RUS	Resonant ultrasound spectroscopy
SEM	Scanning electron microscopy
TEM	Transmission electron microscopy
TZM	Titanium zirconium molybdenum
XRD	X-ray diffraction
YH_x	Yttrium hydride

Report on the Incorporation of Post-Irradiation Examination Results of Yttrium Hydride for Advanced Moderator Handbook

1. INTRODUCTION

Microreactors are small nuclear-fission reactors designed to provide up to approximately 20 MWe power in a passively safe, transportable, and easy-to-deploy package. In order to accomplish these objectives, microreactors must be highly efficient, which necessitates operating at high temperatures. Advanced components must be developed to enable highly efficient and compact microreactors. Accordingly, high-temperature moderators are being developed by the Microreactor Program.

Yttrium hydride (YH_x, where $x < 2$) is metal hydride that has been considered as a high-temperature moderator since the 1950's Aircraft Nuclear Propulsion project [1, 2]. Significant material-property data was obtained through that project and the ensuing decades; some neutron irradiations were even performed using YH specimens. However, limited quantitative information that reports the material properties for neutron irradiated YH_x is available [3, 4]. The U.S. Department of Energy (DOE) Microreactor Program undertook a neutron-irradiation campaign in an effort to investigate the geometric stability, mechanical integrity, and predictable behavior of YH.

This report contains the post-irradiation examination (PIE) results for YH specimens that were fabricated at Los Alamos National Laboratory (LANL) and irradiated in the Advanced Test Reactor (ATR) at Idaho National Laboratory (INL). PIE was performed at the INL Materials and Fuels Complex (MFC). The PIE data will be incorporated in the Advanced Moderator Material Handbook.

2. ATR IRRADITION

The primary variables for neutron irradiation include the specimen's fabrication method and irradiation temperature. Samples were fabricated using a direct massive hydriding method or powder metallurgy, as described in Refs. [5, 6]. Irradiation temperatures of 600, 700, and 800°C were chosen as the relevant low and high temperatures for which YH could be used within microreactors. It was anticipated that little if any hydrogen loss would be observed at 600°C, and more would be observed at 800°C. Finally, the irradiation fluence of $\sim 1 \times 10^{21}$ n/cm^2 was a consequence of reactor constraints. The ATR undergoes a core internal change (CIC) during a substantially long outage period approximately once every 10–12 years. It was highly desirable to complete this YH irradiation before the ATR CIC commenced, which constrained the irradiation fluence to $\sim 1 \times 10^{21}$ n/cm^2.

Details about the LANL-MOD-1 irradiation have been reported elsewhere [7], so a brief summary is provided herein. The LANL-MOD-1 irradiation assembly is shown in Figure 1. A total of 102 YH samples and 36 titanium-zirconium-molybdenum (TZM) foils were irradiated. Samples were irradiated for 60 effective-full-power reactor days. The samples were contained in an e-beam-welded TZM capsule. Two capsules were inside each clam shell, and three clam shells constituted the assembly. A silicon carbide passive temperature monitor and two fluence wires were contained in the center of each clam shell. Two melt wires were included in each of the six LANL capsules.

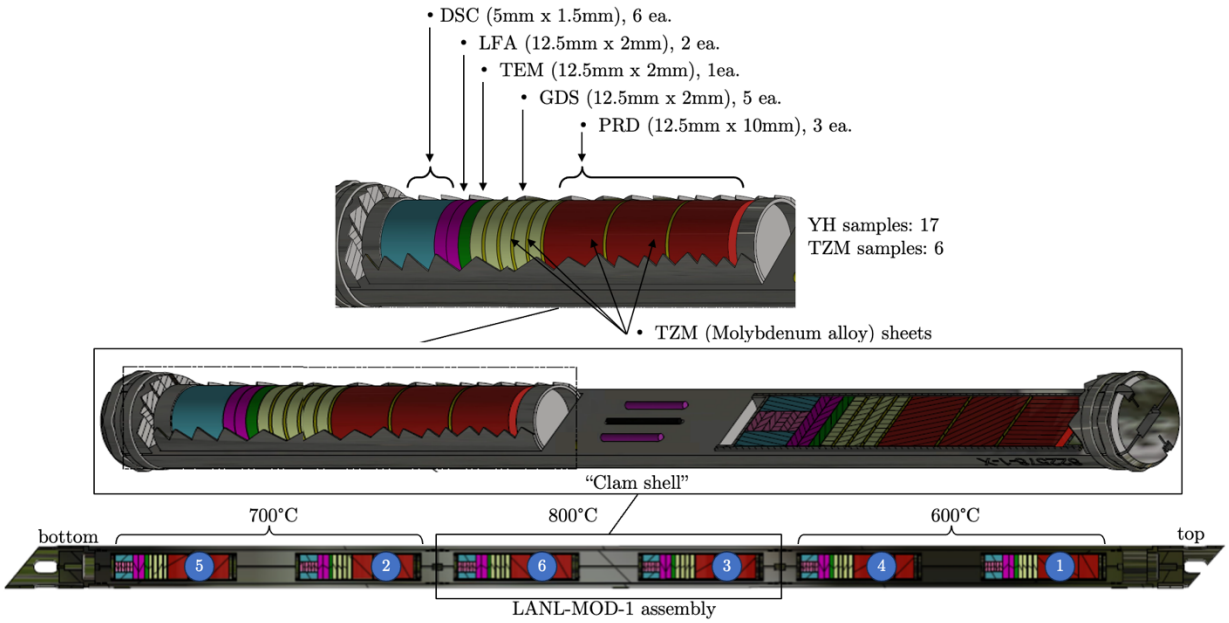

Figure 1. LANL-MOD-1 irradiation assembly.

Sample temperatures were calculated using finite element methods (STAR-CCM+) and neutron fluences were calculated using Monte Carlo N-Particle v5, as shown in Figure 2. In order to achieve the desired capsule temperature, the gas compositions within the individual LANL capsules (displayed per capsule in Figure 2) and within the irradiation assembly (215 torr Ar, 545 torr He) were tailored in combination with the machined gas gaps between the clam shell and the assembly basket. However, Capsule 2B was found to have a crack. The worst-case impacts this crack could have on samples temperatures would occur if the air entrapped in the can was not purgeable. In this potential scenario, after the capsule was sealed, the entrapped air could diffuse and exchange with the capsule-gas mixture and finally reach an equilibrium condition. Because air has lower thermal conductivity, the final conductance of the capsule gap would decrease, which would result in an increase in all the sample temperatures. Each capsule also contained a 10 torr overpressure of hydrogen to discourage hydrogen desorption from the YH samples.

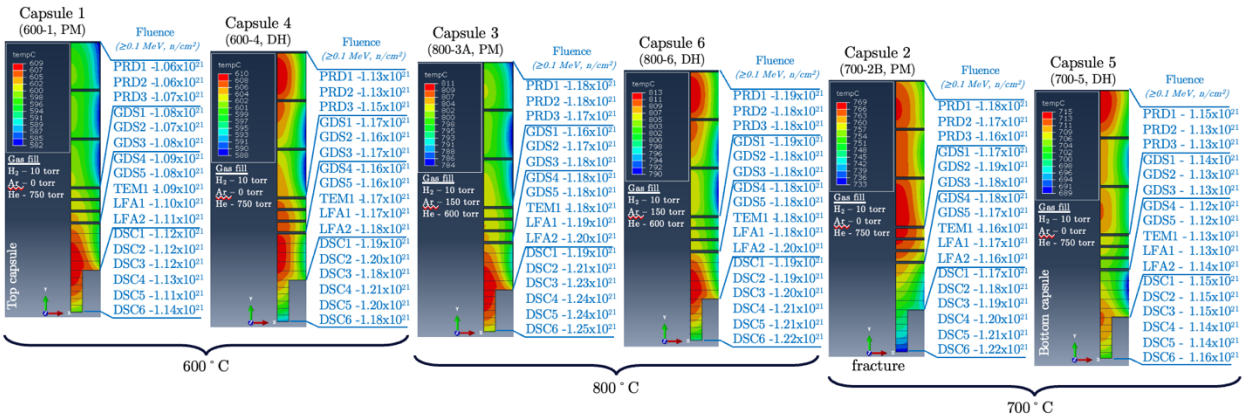

Figure 2. Calculated temperatures and neutron fluences for YH specimens.Temperature profiles are shown in contour plots and fluences are tabulated. Samples in Capsules 1, 3, and 2 were fabricated using powder metallurgy (PM) and 2, 4, 6 using massive hydriding (MH).

3. INITIAL CONDITIONS OF YH_x SPECIMENS

YH_x specimens were manufactured at LANL via MH or adding a powder-compacting step after MH. Further information is available in [5, 6]. Here, the selected as-fabricated specimen pictures are documented to emphasize visible surface-defect features on the as-fabricated specimen surfaces prior to irradiations, as shown in Figure 3. Two types of surface defects were present in some samples as (i) material loss due to surface chips and (ii) discolorations. Most samples exhibited a uniform visual appearance, with no noticeable surface defects—e.g., the Capsule 4 LFA-1 specimen as shown in Figure 3. Some PM-specimen surfaces had significant color variations, ranging from gold, through gray-blue, light-gray, and dark-gray. This type of discoloration was only observed in PM specimens. For massively hydrided specimens, surface discoloration was also present as whitish color, suggesting a surface-oxide formation (see selected specimens from Capsules 5 and 6 in Figure 3).

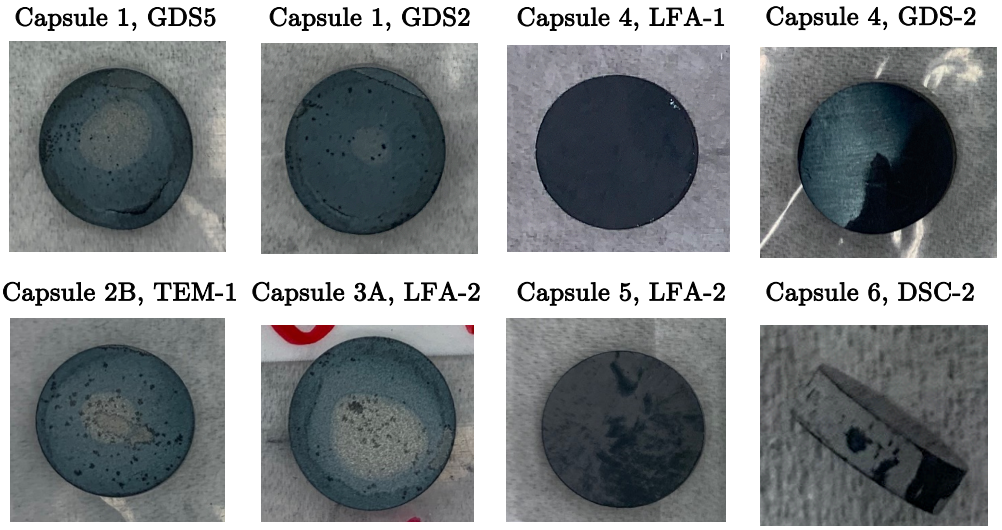

Figure 3. Important surface features of the as-fabricated YH_x specimens prior to irradiation. No scale bar is available.

4. PASSIVE INSTRUMENTATION

This section reports the available passive instrumentation data (fluence wires, melt wires, and SiC thermometry) to determine the irradiation experiment conditions for YH_x specimens.

4.1 Fluence Wires

Three sets of fluence wires were contained within the LANL-MOD-1 irradiation capsule. Detailed analysis of the fluence wires has been provided by Pacific Northwest National Laboratory (PNNL) and included in the PIE documentation. Table 1 shows the fluence-wire results along the ATR reactor elevation at the B2 irradiation position, based on activity measurements. The fast fluence for neutron energies greater than 0.1 MeV was measured as 1.28, 1.40, and 1.27×10^{21} n/cm^2.

Table 1. Fluences levels on the fluence wires as calculated and measured.

Capsule	Modeled fast (>0.1 MeV) fluence ($\times 10^{21}$ (n/cm^2)	Measured fast (>0.1 MeV) fluence $\times 10^{21}$ (n/cm^2)
1 4	1.61	1.28
3A 6	1.71	1.40
2B 5	1.67	1.27

4.2 Melt Wires

Most melt wires were damaged during retrieval. Therefore, limited information was extracted from the melt-wire assessment (see Table 2). The main takeaways from the melt-wire analysis were as follows. The capsules that were expected to be at 610°C likely experienced a radial-temperature-gradient where one side was >630°C and other side was <577°C. Capsules that were expected to be around 810°C experienced higher temperatures, above 865°C. For capsules at 715 and 769°C, no maximum temperature was determined due to lack of melt wires operating around 700°C.

Table 2. Melt-wire examination results: aluminum, silicon, antimony, beryllium, copper, gold, zinc, manganese, and nickel.

Capsule	Average irradiation temperature (°C)	Melting point (°C)	Melt wire	Quartz capsule condition	Qualitative results
1	609	577	88Al 12Si	Intact	No Melting
1	609	630	100Sb	Intact	Melted
4	610	630	100Sb	Intact	Melted
4	610	577	88Al 12Si	Broken	Undetermined
3A	811	865	1.8Be 98.2Cu	Damaged	Likely Melted
3A	811	865	1.8Be 98.2Cu	Damaged	Likely Melted
6	813	865	1.8Be 98.2Cu	Broken	Undetermined
6	813	865	1.8Be 98.2Cu	Broken	Undetermined
2B	769	660	100Al	Broken	Melted
2B	769	681	49Au 16Cu 23Zn 7.5Mn 4.5Ni	Broken	Undetermined
5	715	681	49Au 16Cu 23Zn 7.5Mn 4.5Ni	Intact	Melted
5	715	660	100Al	Intact	Melted

4.3 Silicon Carbide Passive Thermometry

Maximum and minimum irradiation temperatures of the ATR capsule were measured with SiC passive monitors (see Table 3). All irradiated SiC passive monitors were evaluated by optical dilatometry during an isochronal heat treatment. SiC monitors were located between two capsules, as illustrated in Figure 4. At these locations, finite element analysis (FEA)-calculated temperature was higher than the FEA-calculated maximum specimen temperature in the capsules. Therefore, the actual specimen temperature was expected to be lower than the passive thermometry measurements. For 600°C capsules, the linear interpolation predicts the maximum specimen temperature as 574°C. For 700 and 800°C capsules, the predicted specimen temperatures were then 840 and 828°C, respectively.

Noting that all three SiC monitors were chipped during the hot cell disassembly process of the capsules. Because thermometry results were based on the thermal expansion measurements, these minor damages were not expected to impact the thermometry results.

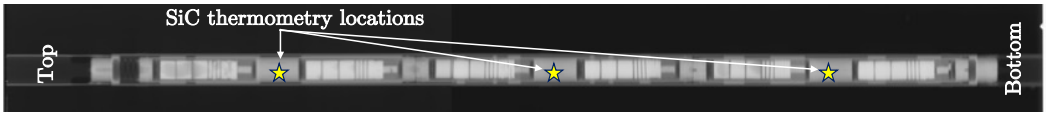

Figure 4. Illustration of the SiC monitor locations in ATR capsules (locations were exaggerated for visibility).

Table 3. SiC temperature monitor results with FEA-calculated target temperatures at location where SiC monitor is present (all temperatures in °C)).

Irradiation Temperature (°C)					
	FEA-Calculated		SiC-measured		Absolute Difference
Sample	At SiC location (Maximum)	Specimen (Maximum)	Minimum	Maximum	|Maximum Target|
1	669	610	590	630	39
2	787	769	850	860	63
3	835	813	810	850	15

5. POST-IRRADIATION EXAMINATION METHODS

This section includes brief descriptions of the PIE methods performed on irradiated YH_x specimens. Detailed information of each technique can be found elsewhere [8, 9].

5.1 Neutron Radiography

Neutron radiography of the ATR capsules consisting of YH_x samples was performed using an indirect technique where the activated dysprosium and indium foils after neutron exposure were placed onto radiation-sensitive x-ray films in a dark room to produce images. Neutron radiography of ATR capsules were collected at 0, 120, and 240 degrees for structural inspection.

5.2 Optical Inspection of Samples

Optical inspections of specimens were performed using a digital microscope. Optical images were collected from front, back, and side of each YH_x disk. The microscope was calibrated using a National Institute of Standards and Technology (NIST)-certified external standard supplied with an uncertainty of ±0.0007 mm.

5.3 Hydrogen Content Measurements

An ELTRA ONH-2000 inert-gas fusion (IGF) analyzer was used for hydrogen measurements. Prior to reference standard and irradiated specimen tests, blank runs with empty tin capsules were performed to evaluate and correct for the hydrogen content of the capsules during data analysis. The instrument was calibrated with NIST-traceable and certified reference standards that have hydrogen contents bounding those predicted for the sample. The calibration runs were then checked by analyzing an independent NIST-traceable certified reference standard with hydrogen content near the middle of the calibrated range. After calibration checks[b], the specimens were tested. An additional check standard run was applied at the end of the sample batch and at least every 1 hour during the analysis to evaluate the detector drift.[c]

The hydrogen concentration of each sample ($[H]_{sample}$) was calculated using Equation 1:

$$[H]_{Sample} = \frac{K_H(A_{Sample} - A_{Background})}{M_{Sample}} \quad (1)$$

where K_H is the sensitivity constant of the instrument for hydrogen, determined through the analysis of a known standard; A_{Sample} is the sample peak area; $A_{Background}$ is the sum of all background contributions to the peak area determined experimentally; and M_{Sample} is the net weight of the sample subtracting out the weight of the capsule. The average hydrogen content is then calculated as the arithmetic mean of a set of individual samples as shown in Equation 2 where $[H]_i$ is the calculated hydrogen concentration for a given sub-sample using Equation 1, and *n* is the number of replicates analyzed.

$$[H]_{Average} = \frac{\sum_{i=1}^{n}[H]_i}{n} \quad (2)$$

5.4 X-Ray Diffraction Analysis

X-ray diffraction (XRD) measurements were performed in a Panalytical Empyrean, equipped with a Pixel 3D detector and using a 0.02 μm Ni filter. The goniometer radius was configured to 240 mm, Soller slits of 0.04 rad, anti-scatter slit of 1/4 degree, and divergence slit of 1.125 degrees (140 mm distant from the sample). Scans were acquired using Cu-Kα radiation, 45 kV and 40 mA, and 2θ ranged from 20 to 140 degrees in Bragg-Brentano geometry, with step size of 0.013 degrees and 200 seconds per step.

Phase identification was carried out in Highscore software from Panalytical, using PDF4+ database from 2023. Rietveld refinements were done with TOPAS software from Bruker, version 4.2. Due to significant grain-size effect on most samples, some crystalline phases were refined with preferential orientation, as supported by the TOPAS software.

5.5 Laser Flash Analysis

Thermal-diffusivity values were measured as a function of temperature using a Netzsch LFA427 instrument inside a shielded glovebox. The samples consisted of cylindrical pellets and their thickness and diameter were measured using Vernier calipers. Each sample was placed in an yttria-painted steel fixture, which was held by an alumina holder, both of which were subsequently placed inside a furnace prior to heating to the desired temperature under high-purity argon (Ar) atmosphere (0.11 MPa). After reaching equilibrium, the front surface of the specimen was subjected to a short laser pulse (0.6–1.2 ms). The rear surface-temperature response was recorded via an infrared detector as a function of time.

b. A check standard passed the analysis when its results were within the 2σ certified value on its certificate.

c. Calibration runs were repeated once the sample results were outside of the calibration range or a check standard sample failed.

5.6 Differential Scanning Calorimetry

DSC traces were measured using a Netzsch DSC 404F1 differential scanning calorimeter using yttria-lined platinum-rhodium crucibles to hold the alloy samples. DSC was measured upon heating and cooling at a rate of 10°C/minute. Ultra-high-purity Ar was used as the cover gas at a flow rate of 20 mL/min after passing it through an oxygen gettering furnace. Oxygen-impurity levels were below parts-per-billion range based on the measured performance of the gettering furnace. All instruments were contained within an Ar atmosphere glovebox with less than 1 part-per-million O_2.

6. CHARACTERIZATION OF IRRADIATED YTTRIUM HYDRIDES

6.1 Neutron Radiography

Prior to capsule disassembly and subsequent destructive examinations, neutron radiography was performed to examine the structural stability of the capsules and specimen. Figure 5 show the neutron radiographs of TZM-cladded YHx specimens in ATR fixture. Radiography was conducted at three different angles of 0, 60, and 120 degrees. The contrast difference in the radiographs was caused by the strength of neutron absorption. Whiter contrast depicts more neutron absorption so that individual YH_x samples were visible with whiter contrast due to a high probability of interaction between matter and incoming neutrons. Other components show gray contrast where neutron absorption was lower than that for YHx specimens. A closer look to the radiographs indicates that some YH_x specimens had contrast variation (see magnified pictures of the regions (orange frames) in Figure 5).

This contrast variation matches with the as-fabricated specimens that had surface discolorations observed visually (see Figure 3), which were likely indicative of oxide formation or H-content (or stoichiometry) variations. Specimens with the contrast variations in the highlighted capsules were prepared by PM.

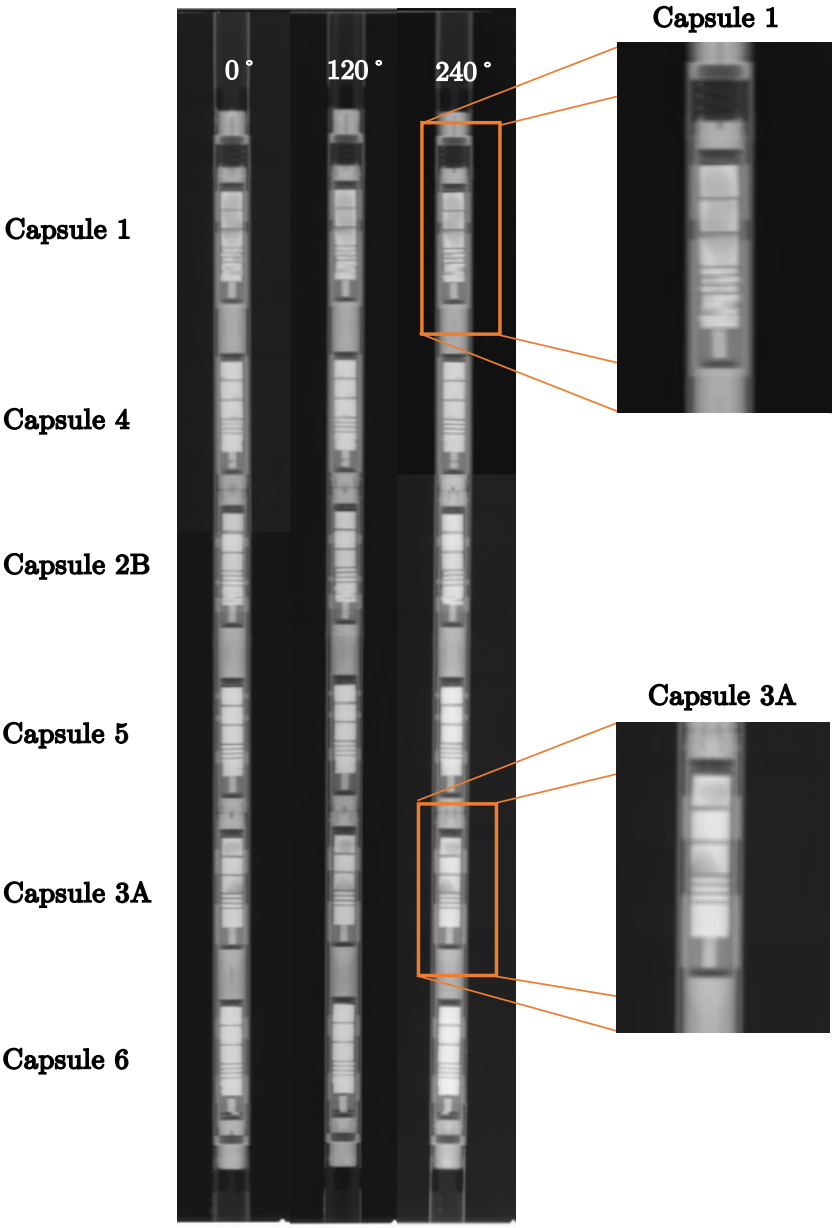

Figure 5. Neutron radiography of the ATR fixture containing TZM-cladded YH_x specimens at angles of 0, 120, and 240 degrees.

6.2 Specimen Integrity During Retrieval

Because YH_x is brittle, one important attribute is its mechanical integrity after irradiation. The neutron radiographs indicated that all samples were intact within the irradiation assembly. Table 4 shows the status of the samples and planned PIE activities after capsule opening is performed using remote manipulators at the Hot Fuels Examination Facility's (HFEF's) main hot cell. When the capsules were opened, several samples mechanically failed prior to being handled with manipulators. Additionally, a few samples bonded to one another. The number of broken, powdered, and bonded specimens were 3, 5, and 6, respectively. For Capsule 3A, bonded specimens were all DSC type, no TZM sheet was present between them. Within this capsule, DSC 1, 2, and 3 were bonded together to form a single specimen while DSC 4 and 5 bonded together, and GDS 5 and LFA 1 samples were broken. GDS specimens of Capsule 600-4, that were fabricated using MH, came out of the capsule as powders. These specimens had TZM sheet between them. Within Capsule 700-5, sample GDS 3 bonded to the adjacent TZM sheet, and DCS5 was broken. In total, 88 of 102 YH_x specimens were retrieved in an intact condition. Additional specimens broke during the inter-facility transfers. Retrieved pieces of an individual broken specimen were used for multiple characterizations, as allowed.

Table 4. The planned PIE activities (color-coded). Capsules 1, 2B, and 3A contained PM specimens, whereas capsules 4, 5, and 6 contained direct massive hydrided specimens.

Capsule Identifications					
600-1	700-2B	800-3A	600-4	700-5	800-6
PRD1	PRD1	PRD1	PRD1	PRD1	PRD1
PRD2	PRD2	PRD2	PRD2	PRD2	PRD2
PRD3	PRD3	PRD3	PRD3	PRD3	PRD3
GDS1	GDS1	GDS1	GDS1	GDS1	GDS1
GDS2	GDS2	GDS2	GDS2	GDS2	GDS2
GDS3	GDS3	GDS3	GDS3	GDS3	GDS3
GDS4	GDS4	GDS4	GDS4	GDS4	GDS4
GDS5	GDS5	GDS5	GDS5	GDS5	GDS5
TEM1	TEM1	TEM1	TEM1	TEM1	TEM1
LFA1	LFA1	LFA1	LFA1	LFA1	LFA1
LFA2	LFA2	LFA2	LFA2	LFA2	LFA2
DSC1	DSC1	DSC1	DSC1	DSC1	DSC1
DSC2	DSC2	DSC2	DSC2	DSC2	DSC2
DSC3	DSC3	DSC3	DSC3	DSC3	DSC3
DSC4	DSC4	DSC4	DSC4	DSC4	DSC4
DSC5	DSC5	DSC5	DSC5	DSC5	DSC5
DSC6	DSC6	DSC6	DSC6	DSC6	DSC6

Color Codes	
	LIBS
	LFA
	DSC
	IGF and XRD (halved samples)

Color Codes
Metallography
Not Available (N/A) due to powdering
PRD (N/A due to dose level)
Reserved samples

6.3 Optical and Metallographic Examinations of Irradiated YH_x Specimens

Optical inspections of each sample were conducted to determine visible moprhological changes or cracks. Importantly, the samples with contrast change were carefully inspected. Instead of providing all the optical pictures of specimens, specimens with important observations were depicted as follows.

A typical irradiated PM-specimen microstructure consists of black pores and dark-gray yttrium oxide precipitates, randomly distributed in the YH_x matrix (gray), as shown in Figure 6.

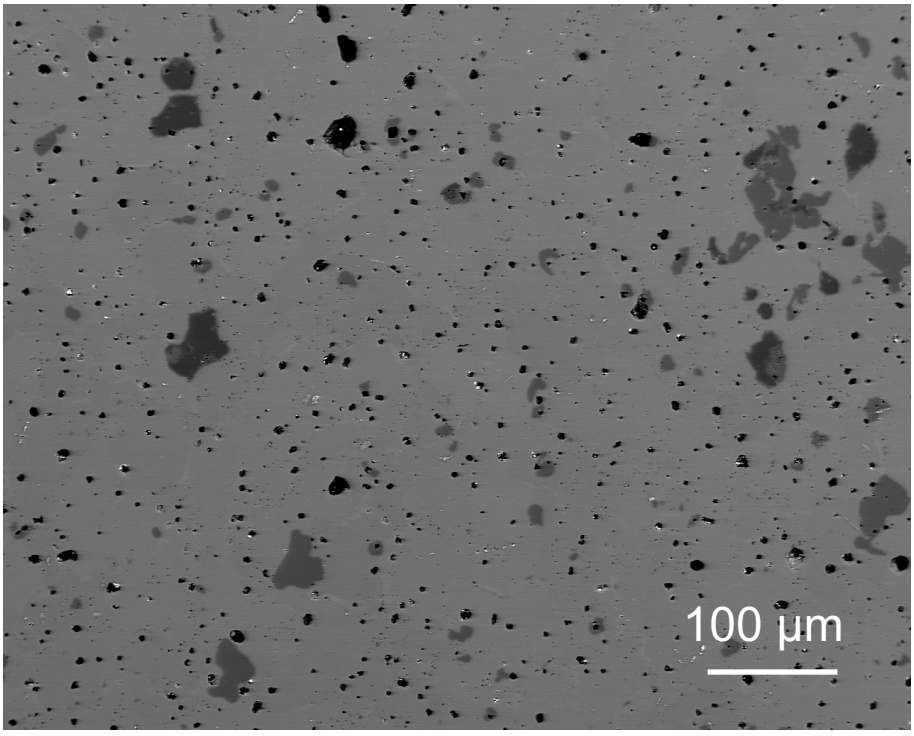

Figure 6. Back scattered electron (BSE) image of an irradiated PM YH_x (Capsule 3A, LFA-1).

For MH specimens, the microstrucutre included no porosity (Figure 7a), and the oxide precipitates were oriented along the grain boundaries, as indicated by the elemental map shown in Figure 7b. The electron backscatter diffraction (EBSD) microscopy revealed the grain microstructure (IPF map of YH_2) where sub-grain formations inside large elongated grains.

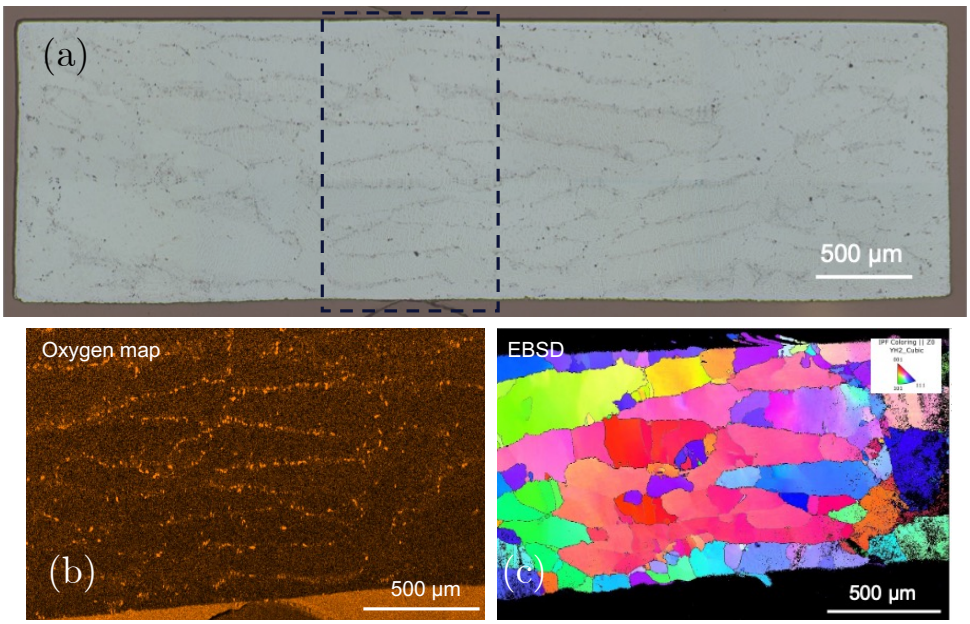

Figure 7. (a) Optical microscopy of the irradiated MH specimen (Capsule 5, DSC-1), (b) oxygen elemental map via energy dispersive spectroscopy (EDS), and (c) the EBSD of the specimen showing the grain-boundary microstructure.

Specimens from Capsule 600-1 had significant color difference ranging from gold, gray-blue, light-gray, and dark-gray, depending on particular lighting conditions. The color alteration was determined to be voumetric, verifiying the radiography data, and not surface limited. Importantly, the comparison of the post- and pre-irradiation pictures of the sample indicated that the size of the discolored regions, in particularly the goldish region, increased. This observation also suggested that hydrogen loss or redistribution could also cause such color alterations. Electron microscopy examination using EBSD showed the majority of grains indexed as YH_x phase, except oxide, yttrium metal, and other precipitates (see Figure 8) which indicates that the color alterations were also related to the grain morphology and potential hydrogen loss, as well as the fabrication step. Noting that, indexing challenges were experienced for Y metal and oxide phases. The black regions of the EBSD micrograph likely correspond to Y-metal and oxide phases. Further elemental analysis at the color-changing regions with EDS detected Mo at noise levels (see Figure 9), which indicates that the discoloration was not due to interdiffusion of Mo from the TZM foils placed between the samples. Oxygen was also observed together with Y, indicating the presence of yttria precipitate, and zirconium was determined to be present in the starting YH_x. Because other specimens in the same capsule and specimens in other capsules had limited color alteration that was confined to surface, it was also considered the the color variations are as a result of the manufacturing process.

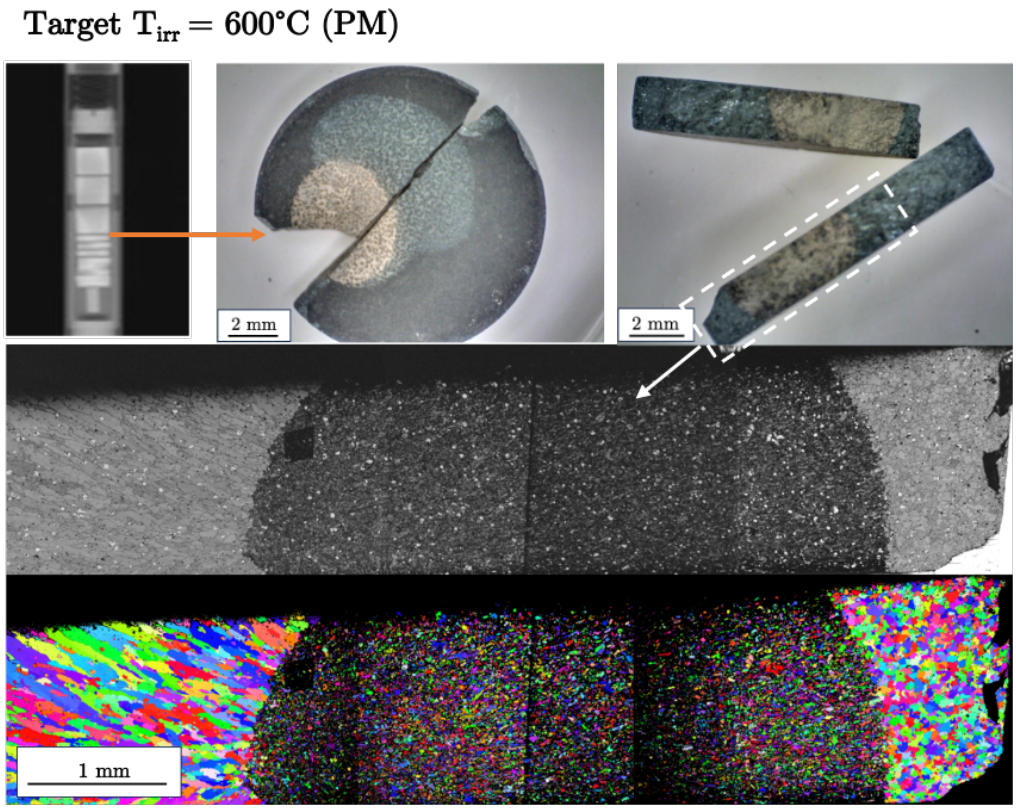

Figure 8. Optical and microscopy examinations of a typical specimen with significant color alteration. EBSD indexed all major grains, except oxides and other precipitates, as YH_x.

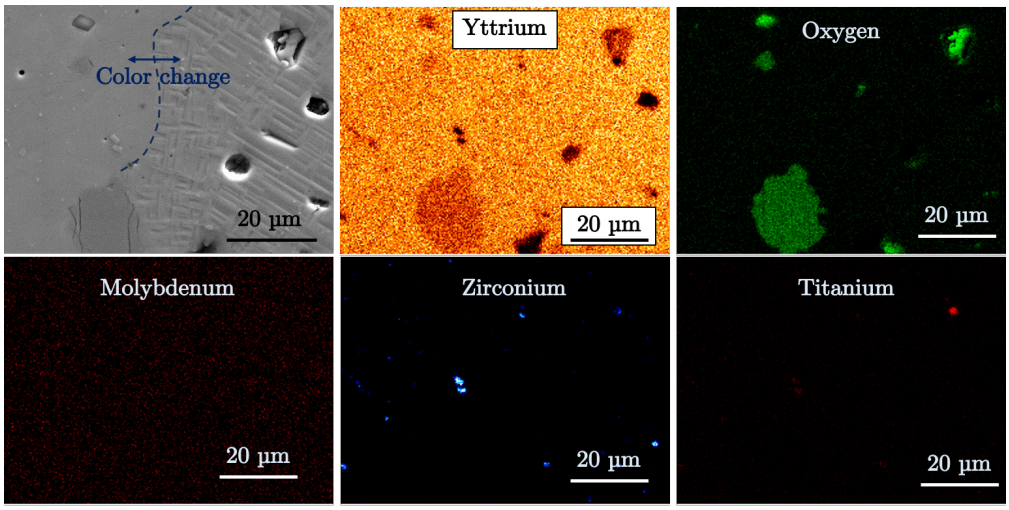

Figure 9. Secondary electron image of the specimen where color change occurs and EDS elemental maps. Mo is at the noise level of the EDS signal.

Overall, small-diameter specimens (shown as DSCs in Table 4) showed better mechanical integrity than the large diameter specimens. DSC specimens of Capsule 800-3A were retrieved as bonded to each other, except one.

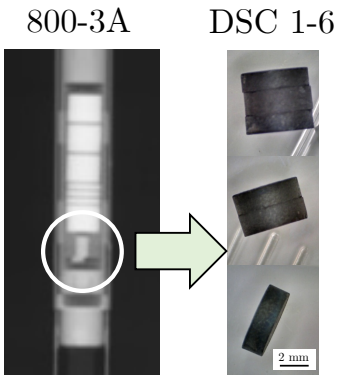

Figure 10. DSC samples of Capsule 800-3A (PM).

6.4 Hydrogen Content Measurements

Hydrogen content of six specimens (color-coded in blue on Table 4) were measured. Two additional samples from the Capsules 700-2B (cracked) and 800-6 (massively hydrided) were tested to assess the impact of pressure-boundary loss and the highest irradiation temperature on hydrogen retention. In total, eight irradiated specimens were prepared at the Analytical Research Laboratory (ARL). After several weeks of air storage, samples were stored in an inert atmosphere as long as possible prior to examinations. However, the Capsule 800-6 GDS 2 sample experienced a significant mechanical degradation during storage. Specimens were sheared into halves. Half of each sample was designated for XRD characterizations for phase identifications. The other halves were used for hydrogen measurements via the IGF technique. Each IGF specimen was crushed, mixed, and sub-sampled six times (replicates). The results of the replicates were used to calculate the average hydrogen concentration for the YH_x disk from which they were taken.

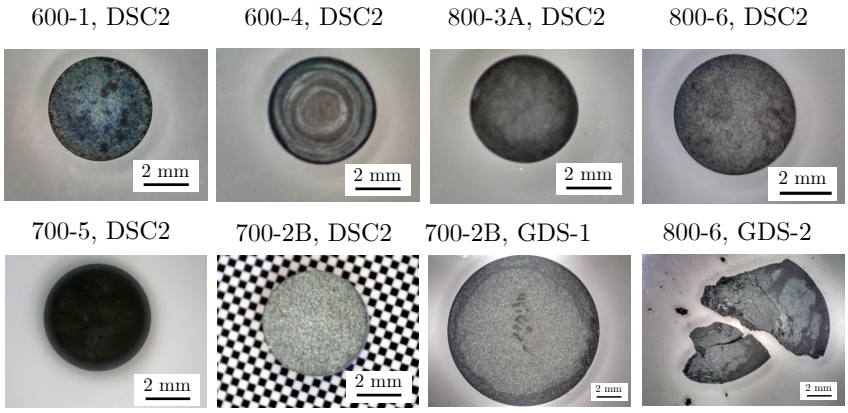

Figure 11. Pictures of the selected samples that were subject to IGF analysis.

Table 5 shows total mass measurements of large specimens and the specimens' average hydrogen content, as determined by IGF. Hydrogen contents of the irradiated samples showed values both lower and higher than the expected approximate value of 21,000 ppm. (Hydrogen content was estimated by considering only Y and H, no O or F was included, therefore actual hydrogen content was expected to be lower than 21000 ppm.) The original hydrogen content for the unirradiated samples was determined by mass measurements. This technique assumes that all mass gain in the sample upon hydriding is due to hydrogen uptake, with no consideration of impurities. Therefore, the uncertainty in these measurements is unknown. The hydrogen content of specimens from Capsules 600-1, 600-4, 700-5, and 800-6 were higher than expected, indicating a stoichiometric increase for those YH specimens. This provided an initial temperature-pressure-composition equilibrium condition that would discourage hydrogen desorption from the YH samples. It is possible that some the H from this overpressure could have absorbed onto some of the YH samples; however, it is unclear why this behavior would not be consistent for all samples. For the 700-2B (cracked) capsules, DSC2 and GDS1 specimens had 15400 and 18200 ppm of hydrogen. For the cracked capsule's specimens, the hydrogen contents were low, as expected, due to hydrogen outgassing from the crack region. The same behavior was also determined for Capsule 800-6 while hydrogen contents of GDS2 and DSC2 sample were determined to be 21200 and 16300 ppm. It is unclear what would cause the hydrogen content in samples within the same capsule to vary so significantly. These results might suggest that some hydrogen was lost either during irradiation or post-irradiation activities. Thus, hydrogen-content measurements of YH were based on what was present after the capsule opening, sample storage, and specimen preparations, as well as the cooling period after irradiation. A scarcity in fabrication details also contribute to the lack of conclusive behavior of the post-irradiated specimens.

Table 5. The mass of large specimens (not replicates) and the average hydrogen content of specimens which were obtained from six replicates from each specimen.

Capsule	Sample	Mass (mg)	Uncertainty (±mg)	As-fabricated H (ppm | H/Y)	H (ppm)	Uncertainty (± %)
600-1	DSC2	17.8	0.2	—	22400 ± 2690 2.0 ± 0.24	12
600-4	DSC2	17.7	0.2	20605 | 1.85	22100 ± 2210 1.98 ± 0.20	10
700-2B	DSC2	17.8	0.2	—	18200 ± 2000 1.63 ± 0.18	11
700-2B	DSC2	17.7	0.2	—	15400 ± 2160 1.38 ± 0.19	14
700-5	DSC2	17.5	0.2	18377 | 1.65	22400 ± 1340 2.0 ± 0.12	6
800-3A	DSC2	18.0	0.2	—	17000 ± 1910 1.52 ± 0.17	13
800-6	DSC2	17.6	0.2	—	16300 ± 1790 1.46 ± 0.16	11
800-6	GDS2	17.9	0.2	20493| 1.84	21200 ± 2970 1.90 ± 0.27	14

6.5 XRD Results

Figure 12 shows the XRD line profiles of specimens from Capsules 600-1 and 4. XRD indicated that YH_2 was the dominant phase, although minor Y-phase is present, as shown in the zoomed section of XRD line profile. Furthermore, multiple minor phases as indexed Y_2O_3 and YOF (not shown in the figures) were determined. Because hydride intensity was significantly higher than the intensity of the Y phase, it could be qualitatively commented that hydrogen loss was minor on these specimens which were irradiated around 600°C.

Figure 13 shows the XRD line profile of specimens in Capsule 800-6. GDS 2 and DSC 2 specimens were at different axial locations in Capsule 800-6. While the normalized intensity of YH_2 peaks were more noticeable than that for Y peaks in the GDS 2 sample, Y-phase peaks were higher than the intensity of the hydride peaks, which insinuated a significant hydrogen loss from that specimen.

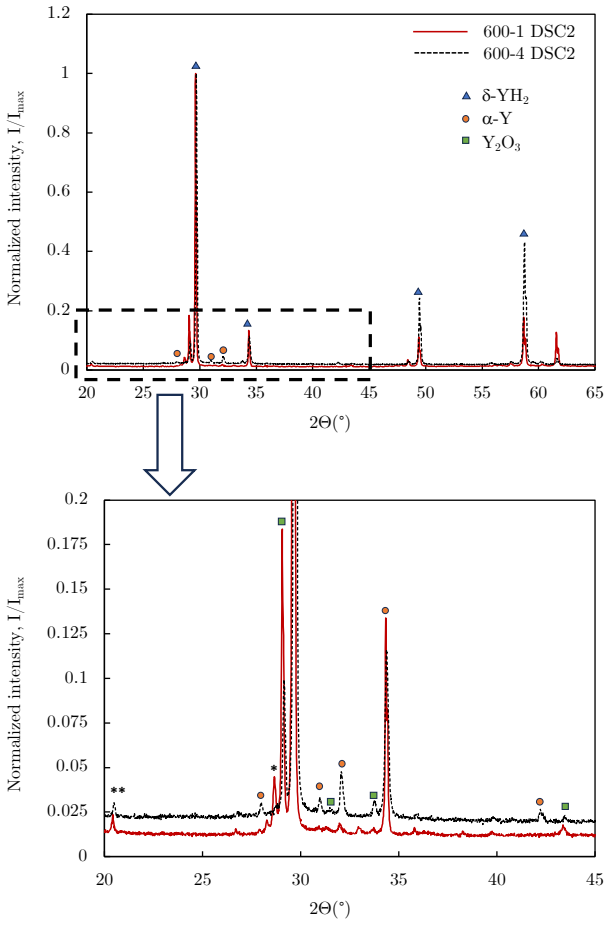

Figure 12. XRD line profile of specimens from Capsules 600-1 and 4.

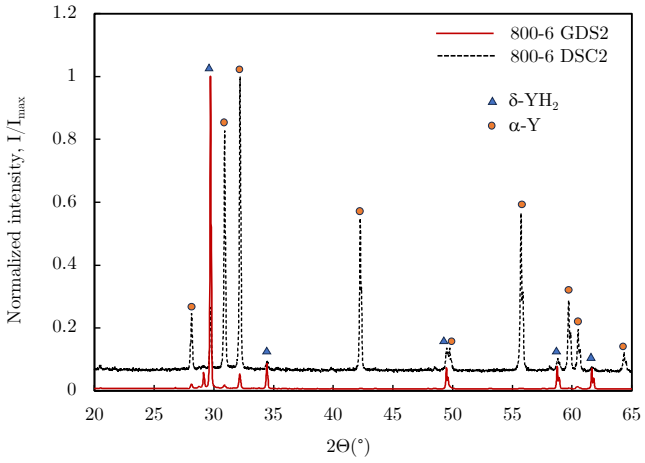

Figure 13. XRD line profile of specimens from Capsule 800-6.

Table 6 summarizes the phase fraction of the main phases as a result of Rietveld refinement as well as the associated hydrogen contents. It should be noted that XRD data originated from a limited volume of material close to the outer surface. Main observations were:

1. Some specimens contained yttrium oxyfluoride (YOF) and yttria (Y_2O_3) phases at unignorable levels. Acknowledging the factors such as the limited x-ray-penetration depth and yttrium oxidation during specimen handling, volume fractions of the second phases show no consistency.
2. For Capsule 600-1 and 4 specimens, the YH_2 phase fraction was significantly higher than that for yttrium-phase fraction, which was an indication of high H retention for 600°C.
3. XRD results of Capsule 800-6 specimens indicated a large H-content variation and a correlated XRD-calculated volume fractions between two specimens taken from different locations. Under the assumption of having similar H stoichiometry, these observations suggested a likely hydrogen redistribution within capsule specimens that were irradiated around 800°C.
4. Specimens from the cracked capsule (i.e., 700-2B) had lower H content and consistent XRD volume fractions of phases.

Table 6. Hydrogen content of the specimens and XRD with the estimated volume fractions of important phases.

						XRD Volume fractions (%)			
Capsule	Sample	T (°C)	Fabrication	Initial H (ppm)	Final H (ppm)	YOF	Y_2O_3	Y	YH_2
600-1	DSC2	600	PM	—	22400	11.01	11.98	2.42	73.38
600-4	DSC2	600	MH	20605	22100	0.13	16.41	9.28	74.18
700-2B	DSC2	800	PM	—	18200	2.40	6.19	23.58	67.04
700-2B	GDS2	800	PM	—	15400	0.86	21.52	23.97	53.41
700-5	DSC2	800	MH	18377	22400	0.90	3.40	45.81	49.90
800-3A	DSC2	800	PM	—	17000	4.85	32.87	12.08	49.23
800-6	DSC2	800	MH	—	16300	1.03	0.98	79.15	18.83
800-6	GDS2	800	MH	20493	21200	3.40	2.10	14.65	79.08

6.6 THERMAL PROPERTIES

LFA and DSC measurements were performed on ATR-irradiated YH_x specimens, as depicted in Table 4, to determine the thermal diffusivity (a) and heat capacity (cp). These measurements were not taken under hydrogen partial pressure by following the pressure-concentration-temperature curves. The LFA and DSC results should not be treated as an absolute YH_x property measurement. For each specific moderator environment, LFA and DSC results may differ. Because LFA and DSC measurements were taken up to 800°C, hydrogen loss was expected to change the specimen stoichiometry and, thus, the collected data. This enabled the study to track the hydrogen loss via thermal-property signature.

6.6.1 LFA Measurements of ATR-Irradiated Yttrium Hydrides

The thermal-diffusivity values (mm^2/s) of fresh and irradiated YH discs are shown in Figure 14 through Figure 16 for samples irradiated at target temperatures of 600, 700, and 800°C, respectively. Main observations were:

1. Irradiated-specimen thermal diffusivity was lower than the fresh-specimen thermal diffusivity, which is likely related to the stoichiometric change as a result of hydrogen loss during irradiation and following examination steps. Because initial stoichiometry of initial samples was not available, the amount of hydrogen loss was unclear. In addition, the thermal diffusivity of hydrogen-free irradiated yttrium metal and the effect of defect recombination is unknown.
2. All specimens, except the fresh one, at elevated temperatures (600–800°C) had similar thermal diffusivity, which was independent of stoichiometry.
3. PM-prepared specimens that were irradiated at 600°C showed an increase in thermal diffusivity during the cooling run from 800°C, which could be associated with the reabsorption of trapped hydrogen in the closed pore structures or networks. PM samples irradiated at 800°C (e.g., Capsules 7B and 8) did not follow this trend, likely due to significant hydrogen loss as compared to specimens irradiated 600°C. Noting that, the pressure boundary of Capsule 7B was not intact.
4. Direct MH specimens showed no difference in their heating and cooling runs, which would be an indication of minimal hydrogen loss.

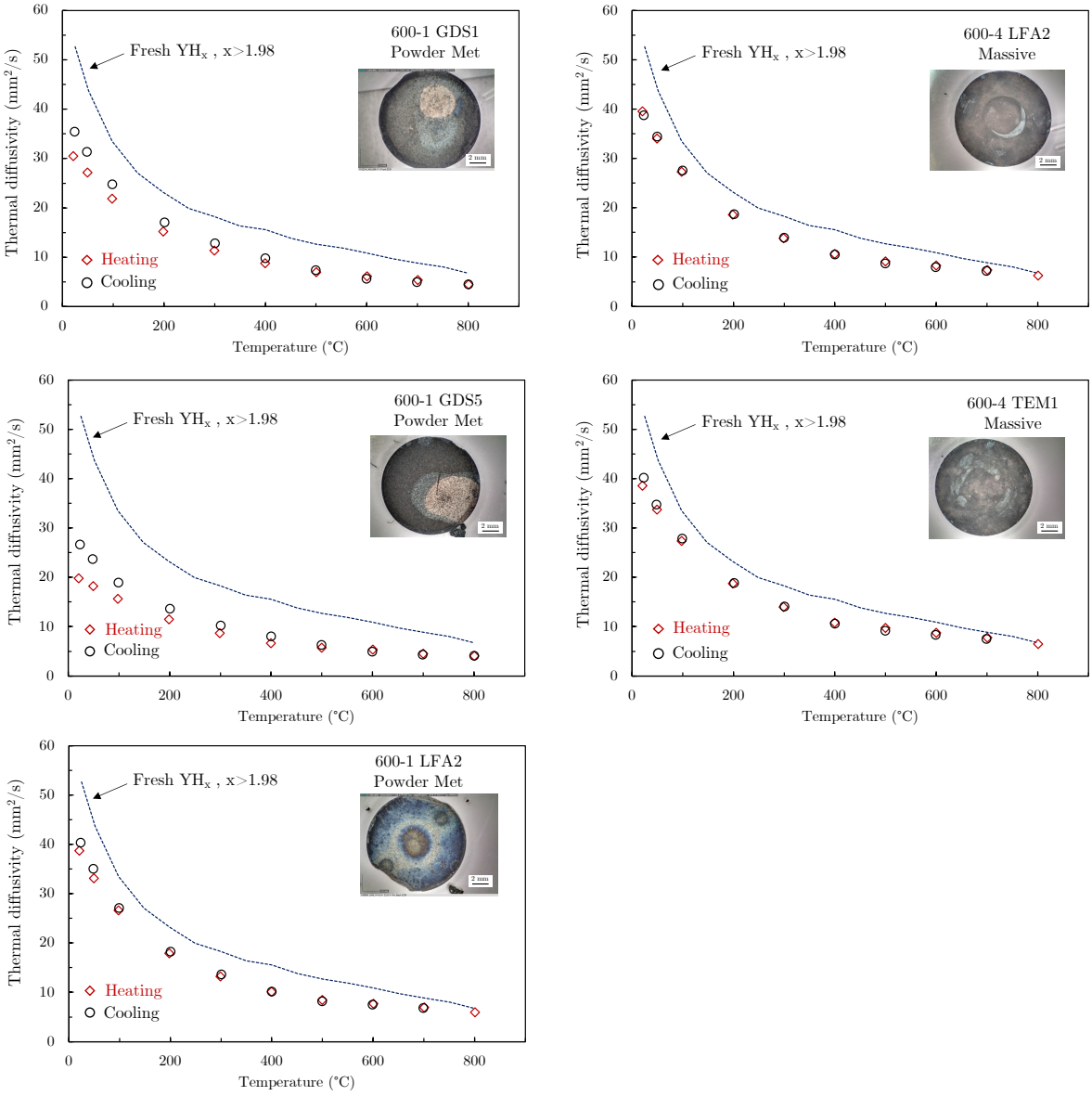

Figure 14. Thermal diffusivity of YH_x specimens irradiated at 600°C.

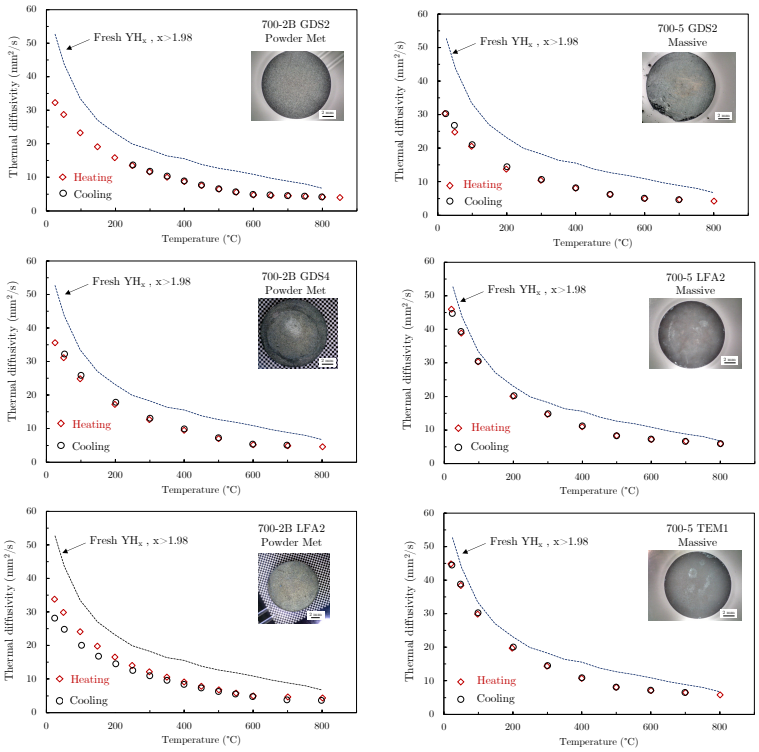

Figure 15. Thermal diffusivity of YH_x specimens irradiated at 700°C (target temperature).

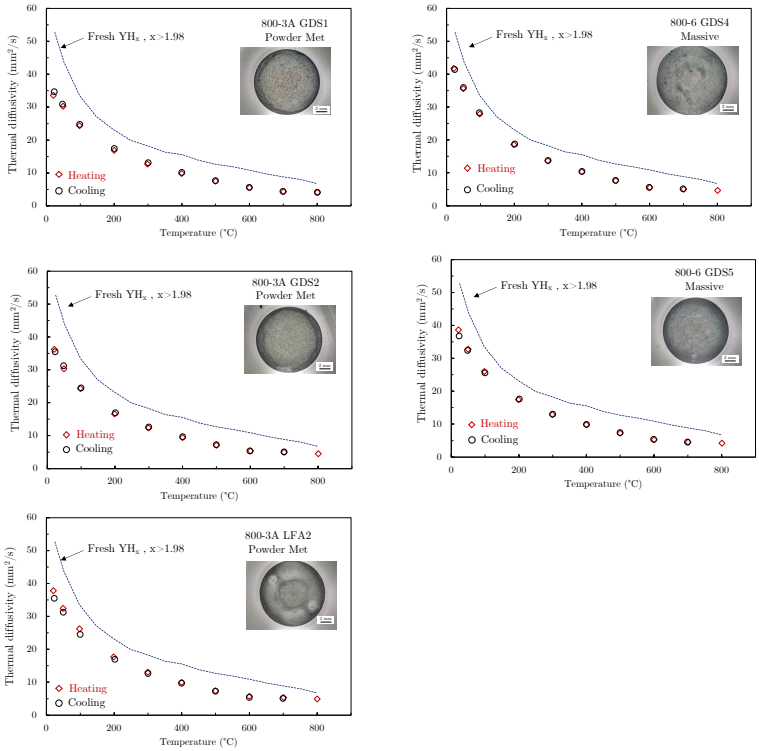

Figure 16. Thermal diffusivity of YH_x specimens irradiated at 800°C (target temperature).

Table 7. Capsule-averaged thermal diffusivity of irradiated samples. Diffusivity was fit to a function of 1/(A+BT).

Capsule	Fabrication method	Target T_{irr} (°C)	A (s/mm^2)	B (10^{-4} Ts/mm^2)
600-1	Powder met	600	0.0224	2.3970
600-4	Massive	600	0.0216	1.6759
700-2B	Powder met	700	0.0068	2.9842
700-5	Massive	700	0.0170	2.2318
800-3A	Powder met	800	0.0112	2.6469
800-6	Massive	800	0.0065	2.7383

6.6.2 DSC Measurements of ATR-Irradiated Yttrium Hydrides

This section includes a typical DSC signal of an irradiated specimen (see Figure 17) and main observations for discussion. DSC signal of the fresh YH_x with x value close to 2 exhibits a smooth, monotonically increasing behavior during heating to 800°C. At this temperature, the rate of H loss increases, and H/Y ratio decreases (see also hydrogen-desorption data [10]). With the start of the cooling at 800°C, effect of the H/Y ratio is manifested as a sudden decrease in the DSC signal. For subsequent heating cycles, the same effect is observed as a sudden increase in the DSC signal too. Furthermore, the peak temperature during sudden change is a function of stoichiometry [11]. Therefore, DSC signals, as well as other thermal-property measurement techniques, contain a signature related to H/Y ratio or stoichiometry. This observation emphasizes the importance of careful use of thermal-property data of YH_x in fuel-performance codes.

Figure 17 depicts the DSC data of direct-hydrided specimen irradiated at target temperature of 600°C. DSC signal consistently shows the effect of the hydrogen loss from YH_x via a shift on the local peak temperature where sudden change occurs, as described above.

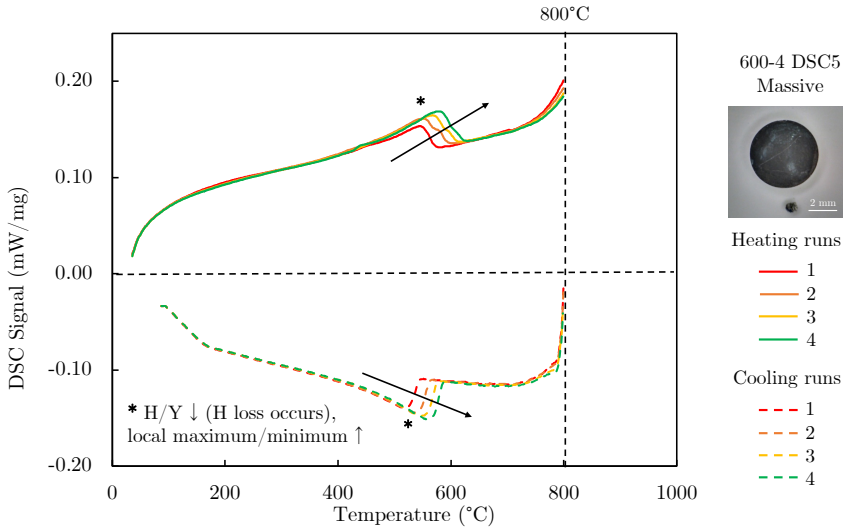

Figure 17. A typical DSC signal from irradiated YH_x.

7. CONCLUSIONS AND FUTURE WORK

This report includes a summary of the YH_x PIE data and comprehensive data sets have been provided to LANL to be incorporated into the Advanced Moderator Handbook. PIE activities aim to understand the solid moderator's high-temperature irradiation performance from the perspectives of geometrical stability, mechanical integrity, and predictable behavior. The behavior of hydrogen in YH_x was investigated with hydrogen-content measurements and XRD. Furthermore, thermal-property measurements and metallography were performed to qualitatively investigate behavior of hydrogen in YH_x. The passive temperature measurements suggested that the 700°C-capsules (Capsules 2B and 5) experienced higher temperatures (above 800°C) than the target temperature of 700°C. Thus, only two temperature conditions (600 and 800°C) may have been met during the ATR irradiation.

Prior to the dismantling of the irradiation assembly, the geometrical stability and mechanical integrity of all YH_x specimens were almost preserved with a couple of exceptions, based on neutron-radiography data. Due to the brittle nature of YH, some specimens lost mechanical integrity during specimen retrieval, handling, and transportation.

Neutron radiography also qualitatively revealed H distribution by contrast variations. These contrast variations were observed in some samples with optical and electron microscopy where the grain morphology abruptly changes. Thus, the visible color alterations in the specimens were deduced to be a result of grain morphologies and H loss. Hydrogen-content measurements and XRD results showed fair correlation. However, limited information on the initial stoichiometry of specimens confounded solid conclusions on hydrogen's behavior. Thermal properties of YH_x specimens exhibited signatures on the H loss or regain where the stoichiometry impact was visible. All these methods show potential as a metric for the assessment of irradiated YH_x.

For 600°C, H is expected to be mostly retained in the YH_x phase, based on results of hydrogen content, XRD, and thermal diffusivity. The cladding will provide an additional containment at this temperature. For 800°C, a portion of H will be contained in the YH_x matrix, but cladding with high H-permeation resistance will be needed to extend the operation temperature.

The manufacturing readiness of YH_x prior to irradiation is critical for YH_x qualification and accurate determination of operating conditions. Thus, systematic irradiations that include the essential parameters, such as time, fluence, temperature, and stoichiometry, are a need to finalize medium technological-readiness levels for the use of YH_x as moderator.

8. REFERENCES

[1] J.P. Blackledge, Chapter 5 - Chemistry of Metal Hydrides as Related to Their Applications in Nuclear Technology, in: W.M. Mueller, J.P. Blackledge, G.G. Libowitz (Eds.), Metal Hydrides, Academic Press1968, pp. 119-164.

[2] W.M. Mueller, Chapter 2 - Hydrides in Nuclear Reactor Applications, in: W.M. Mueller, J.P. Blackledge, G.G. Libowitz (Eds.), Metal Hydrides, Academic Press1968, pp. 21-50.

[3] J.C. Marshall, R. Van Houten, W.G. Baxter, 1000 Hour demonstration of clad yttrium hydride as a neutron moderator in: M. Ferrier (Ed.) American Nuclear Society 1964 annual meeting, America Nuclear Society, Inc., Philedelphia, 1964, p. 2.

[4] J.C. Marshall, R. Van Houten, W.G. Baxter, Yttrium hydride moderator evaluation — in-pile thermal stability, United States, 1962.

[5] A.P. Shivprasad, J.R. Torres, T.E. Cutler, J.K. Jewell, V.K. Mehta, S. Widgeon Paisner, C.A. Taylor, C.N. Taylor, H.R. Trellue, D.W. Wootan, E.P. Luther, Advanced Moderator Material Handbook (FY22 Version: Revision 2), United States, 2023, p. Medium: ED.

[6] A.P. Shivprasad, D.M. Frazer, V.K. Mehta, M.W.D. Cooper, T.A. Saleh, J.T. White, J.R. Wermer, E.P. Luther, D.V. Rao, Elastic moduli of high-density, sintered monoliths of yttrium dihydride, Journal of Alloys and Compounds 826 (2020) 153955.

[7] H. Trellue, C. Taylor, E. Luther, T. Cutler, A. Shivprasad, J.K. Jewell, D.V. Rao, M. Davenport, Advancements in Yttrium Hydride Moderator Development, Nuclear Technology 209(sup1) (2023) S123-S135.

[8] M. Cinbiz, J.A. Charboneau, I.M. Hobbs, G.C. Papaioannou, T.A. Johnson, L.A. Hone, S.C. Middlemas, C.N. Taylor, Initial Post Irradiation Examination of Irradiated Yttrium Hydride (INL RPT-22-68084 FY22 Revision 0), Idaho National Laboratory, Idaho Falls, 2022.

[9] M.N. Cinbiz, J.A. Charboneau, I.M. Hobbs, T.A. Johnson, C.N. Taylor, Report On Hydrogen Content Measurements of Yttrium Hydrides, Idaho National Laboratory (INL), Idaho Falls, ID (United States), 2023.

[10] X. Hu, D. Schappel, C.M. Silva, K.A. Terrani, Fabrication of yttrium hydride for high-temperature moderator application, Journal of Nuclear Materials 539 (2020) 152335.

[11] A.A. Trofimov, X. Hu, H. Wang, Y. Yang, K.A. Terrani, Thermophysical properties and reversible phase transitions in yttrium hydride, Journal of Nuclear Materials 542 (2020) 152569.